Supplementary Information for:

A Versatile Method for the Determination of Photochemical Quantum Yields via Online UV-Vis Spectroscopy

Eduard Stadler,[a] Anna Eibel,[a] David E. Fast,[a], Hilde Freißmuth,[a] Christian Holly,[a] Matthias Wiech,[a] Norbert Moszner[b] and Georg Gescheidt[a]*

[a]Institute of Physical and Theoretical Chemistry, NAWI Graz, Graz University of Technology, Stremayrgasse 9, 8010 Graz, Austria.

[b]Ivoclar Vivadent AG, Bendererstrasse 2, 9494 Schaan, Liechtenstein.

E-Mail: g.gescheidt-demner@tugraz.at

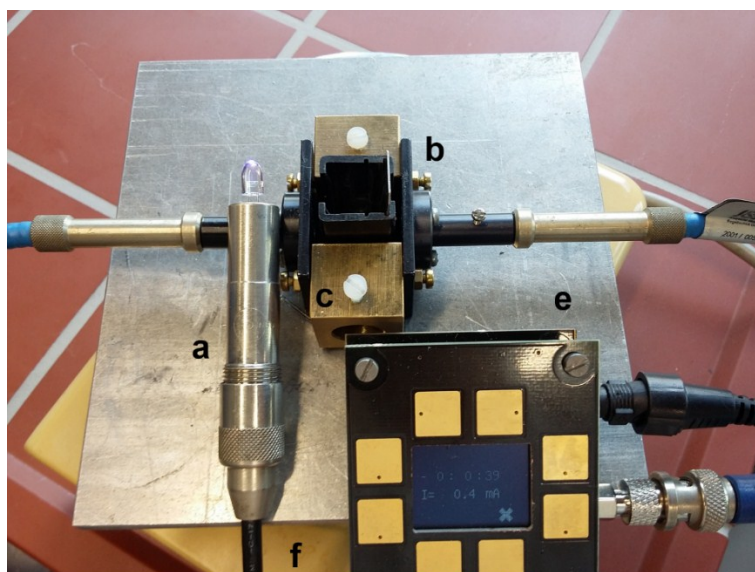# Contents

Sample irradiation

Fig. S1. Setup used for this study. LED, LED-holder and cable (a, detached from cuvette holder for visibility), modified sample holder with optical fibers of the spectrometer (b), LED aperture with plastic screw for fixation (c), custom-made LED driving device (e) used for setting the forward current and illumination time and magnetic stirrer (f).

The photon flux was measured with a calibrated spectrophotometer, equipped with an integrating sphere. The measurement conditions were designed to match the irradiation conditions in the photo-reactor (Fig. S2, left). To obtain the photon flow, the spectra were integrated numerically and the obtained optical output power (in mW) was converted to a photon flux by using Equation 2 of the main text. An example of spectra from a single 385 nm LED operated at different forward currents are shown in Fig. S2 (right).
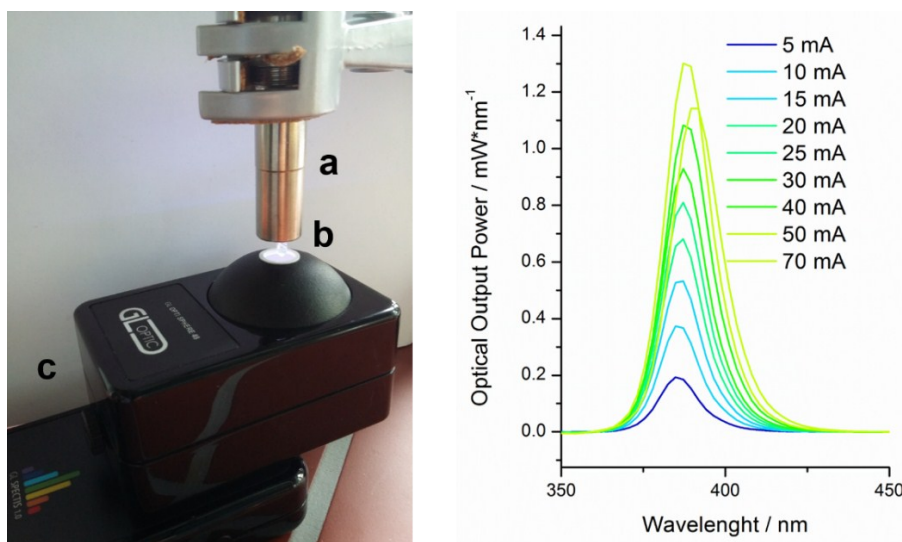
Fig. S2. Left: Setup for LED light intensity measurement: LED holder with LED (a), Ulbricht sphere with 9 mm aperture (b) and spectrophotometer (c). Right: Optical output power per nm (in units of mW) vs. the wavelength (in nm).

We assessed possible intensity losses of the irradiation beam by a control experiment. A green LED (type 490-06) was operated at a low driving current (1 mA) and the detector of the spectrometer was mounted on the opposite side of the cuvette. To prevent overloading the detector we inserted a piece of paper between cuvette holder and detector. The measurement geometry is shown in Fig. S3.
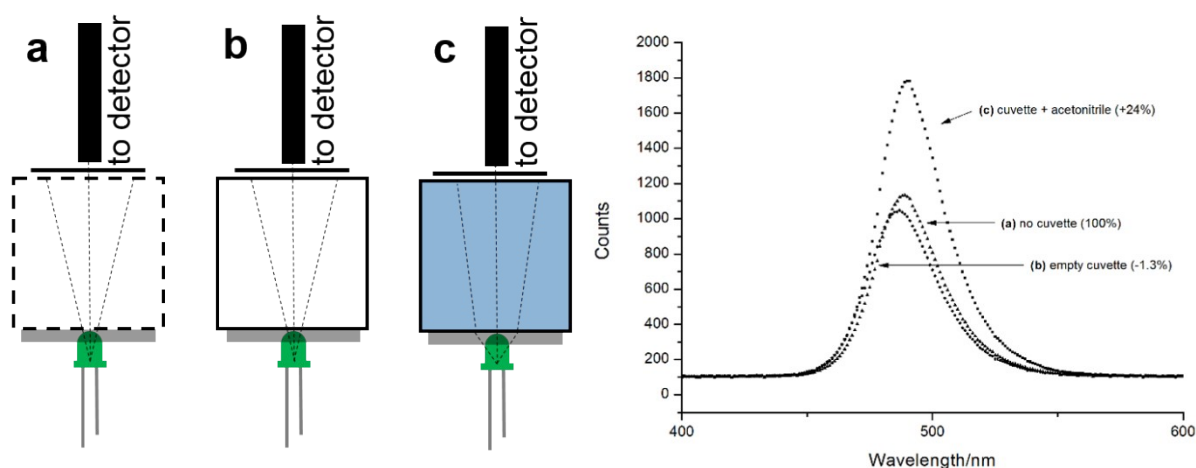

Fig. S3. Control experiment performed with green LED (LED 490-06). The measurement was conducted with no cuvette inserted to the sample holder (a, integral set to 100%), with an empty cuvette in the sample holder (b, -1.3%) and with a cuvette filled with acetonitrile (c, + 24%).

Saturating the measurement solutions with argon can result in a significant reduction of sample volume due to solvent evaporation. Single absorbance spectra of the samples measured before and after the degassing process may be used to correct

these effects. The corrected volume (V_2) is computed from the absorbance values at any local maximum (A_1, A_2) and the deployed volume (V_1) according to Equation S1.

$$V_2 = \frac{A_1}{A_2} * V_1$$

(S1)

We selected different LED types (Table S1) and assessed their suitability for actinometric measurements. The LEDs were placed in front of the aperture of the spectrophotometer (Fig. S2) and the current varied from 5 mA to 70 mA. To allow temperature equilibration the LEDs were switched on for 20 s before each measurement. The graphical representation of the optical output power *vs.* the forward current is shown in Fig. S4. All LEDs display a broad linear range, typically ranging up to 40 mA forward current. Beyond this current, the optical output power loses its linear dependence on the forward current and the standard deviation rises. The results together with the standard deviation between different LEDs of the same type (n = 6) are listed in Table S1.
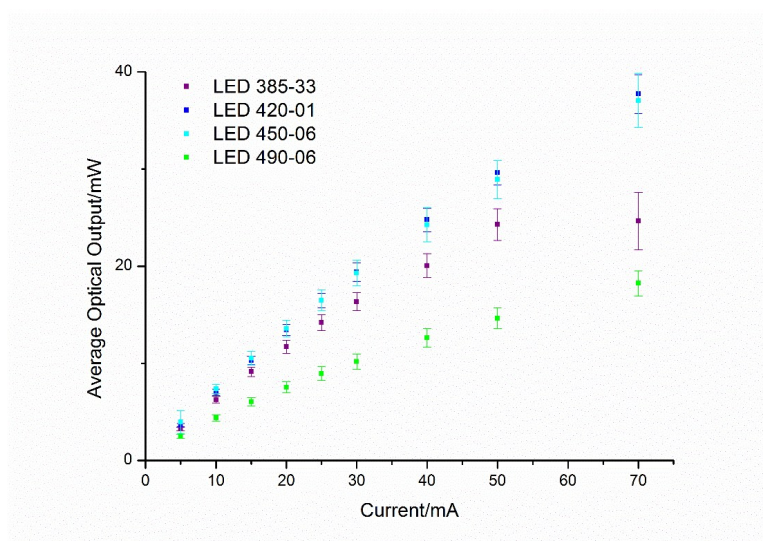

Fig. S4. Average optical output power (n = 6) of different LEDs plotted against the applied forward voltage.

Table S1. Optical output powers of four different LED types emitting from 385 nm to 490 nm at different forward currents. The first column are values obtained with the LEDs used in this study (bold heading). The standard deviation is also listed (n = 6).

Forward Current [mA]	385-33 [mW]	420-01 [mW]	450-06 [mW]	490-06 [mW]
5	3.2 ± 0.2	3.6 ± 0.1	4.0 ± 0.3	2.5 ± 0.2
10	6.3 ± 0.3	7.0 ± 0.3	7.4 ± 0.5	4.4 ± 0.3
15	9.1 ± 0.5	10.3 ± 0.5	10.5 ± 0.7	6.0 ± 0.4
20	11.7 ± 0.6	13.4 ± 0.6	13.6 ± 0.9	7.5 ± 0.6
25	14.2 ± 0.8	16.5 ± 0.8	16.5 ± 1.1	9.0 ± 0.7
30	16.3 ± 1.0	19.4 ± 0.9	19.3 ± 1.3	10.2 ± 0.8
40	20.1 ± 1.2	24.8 ± 1.2	24.3 ± 1.8	12.6 ± 1.0
50	24.3 ± 1.6	29.6 ± 1.3	28.9 ± 2.0	14.6 ± 1.1
70	24.6 ± 2.9	37.7 ± 2.0	37.1 ± 2.8	18.2 ± 1.3

Theoretical background

In this section the use of mono-exponential function for data analysis is justified. In case of a weakly absorbing solution ($A_i^{'}$ < 0.1) the light absorbed by the reactant can be approximated by a linear function, *i.e.* it changes linearly with the reactants concentration. In this case Equation 3 of the main text can be approximated as

$$\frac{d[R]}{dt} = -I_{Abs.}^{R}\Phi \approx -K[R]\Phi \tag{S2}$$

with K being a constant factor that does not change during the reaction. This equation can be integrated and yields the commonly encountered apparent first order kinetic behavior of photo-reactions.

$$[R](t) \approx c_0 e^{-kt} \tag{S3}$$

Thus, we fit the data with a mono-exponential function of the form $y = y_0 + Ae^{-kt}$ with y_0 being the offset ($= A^{\infty}$), A the amplitude of the function ($= A^i - A^{\infty}$) and k the decay constant ($= k_{fit}$ in s^{-1}), respectively. Altogether this yields

$$A(t) = A^{\infty} + (A - A^{\infty})e^{-k_{fit}t} \tag{S4}$$

The derivative of this function at *t = 0* where $A = A^i$ is given as

$$A^{'}(0) = -k_{fit}(A^i - A^{\infty})e^{-0} \tag{S5}$$

This expression is combined with Equation 6 in the main text, eventually leading to Equation 8 that is used for determining the quantum yield.

In the following we seek to determine when the above stated linear relationship between conversion and light absorbed by the reactant is observed. The absorbance at the irradiation wavelength ($A^{'}$) during the reaction as a function of the conversion ξ is given as

$$A^{'} = (1 - \xi)A_i^{'} + \xi A_{\infty}^{'} \tag{S6}$$

For instance, consider a photochemical reaction carried out in a cuvette with d = 1 cm starting with $A_i' = 1$ and ending with $A_\infty' = 0.25$. Obviously, the extinction coefficient of the product (or several products in case of photoinitiators) is 25% of the initial compound. Therefore, the reactant will only absorb a fraction of the total absorbed light as the reaction proceeds. This fraction is expressed in Equation S7.

$$\frac{I_{Abs.}^R}{I_0} = \left(1 - 10^{A'}\right)\frac{(1-\xi)A_i'}{A'} = F(1-\xi)A_i'$$

(S7)

Here F is the photokinetic factor, $F = (1 - 10^{-A'})/A'$. Fig. S5 shows a plot of $I_{Abs.}^R/I_0$ vs. the conversion, ξ for different sets of A_i' and A_∞'. In the case of apparent first order kinetics the data calculated with Equation S7 lie close to a straight line which is indicated by the R-squared value. High initial absorbance at the irradiation wavelength in general reduces the validity of the model (low R^2, e.g. entry A). In general, reducing the concentration results in higher linearity (compare A with entry B and C with entry B). However, overestimation of the absorbed light by the reactant in the initial and final phase and underestimation in the middle are still visible. An example for this situation is given in Fig. S6 where compound **4** (for details see chapter "Cleavage of photoinitiators (4 and 5)") was irradiated with $A_i' = 0.6$. In this concentration fitting to a mono-exponential function may lead to systematic deviations. When a smaller concentration is used and hence $A_i' < 0.1$ the residuals show a random distribution (see Fig. S22 in the same chapter). When the photoproduct absorbs, linearity increases as well (compare entry A with C and F) because the photokinetic factor stays constant during the reaction. High absorbance leads to a saturated region, as encountered in entry E. A severe inner filter effect is shown in entry G which essentially reverts the situation shown in entry C. Dilution again leads to increased linearity (entry H).
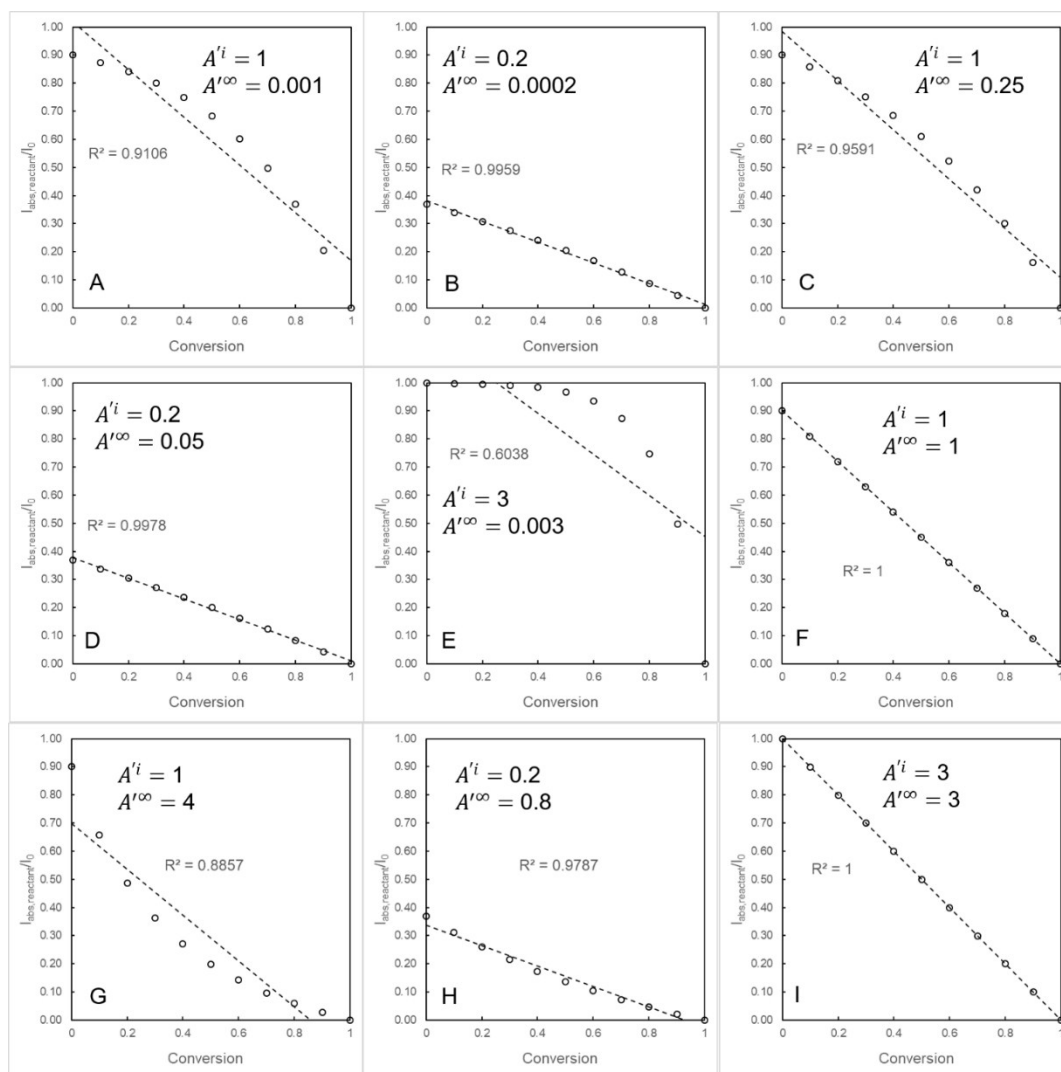
Fig. S5. Fraction of light absorbed by the reactant of a photo-reaction as a function of the conversion. The data were calculated with Equation S7.
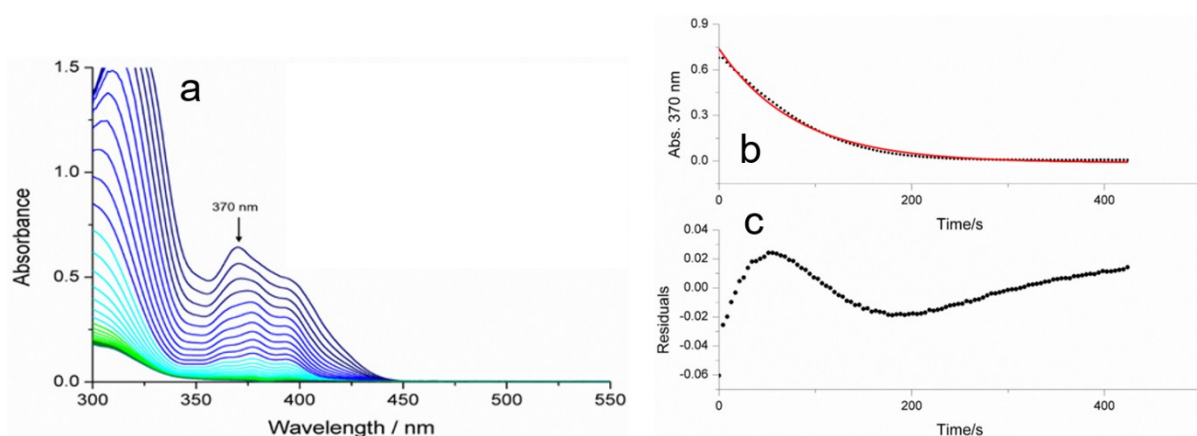

Fig. S6. Spectral changes observed upon irradiation of **4** with $A_i^{'} \sim 0.6$ (time steps between each spectrum: 12 s) (a). b shows the decay of the absorbance at 370 nm vs. the irradiation time and a mono-exponential fitted curve. The residuals are shown in c. (Sample: 1.1 mM **4** in acetonitrile/MMA (1/1 v/v).)

We recommend to always adjust the absorbance of solutions to values below 0.1 in the cases where a mono-exponential function is used for data analysis. A solution with $A'_i = 0.1$ absorbs 20.57% of the incident light (calculated as $1 - 10^{-A}$). Using a linear function obtained by a linear least square fit of data obtained by Equation S7 and assuming $A'_\infty = 0.001$ (intercept = 0.2091, slope = − 0.2055, R^2 = 0.9989) to calculate the absorbed light gives 20.91%. The deviation at the beginning of the reaction is therefore 1.7%, which is below 2%.

To verify the above discussion experimentally we used ferrioxalate solutions (compound **2** see chapter "Actinometric measurements using ferrioxalate (**2**)") at different concentrations and hence different absorbances at the irradiation wavelength. Starting from a concentrated solution with $A'_i =$ 3 showing an initial linear phase ("a" in Fig. S7 and S8) we reduced the concentration to achieve $A'_i =$ 0.1 that is well described by a mono-exponential function (entry "e" in Fig. 7 and 8). The linear region can be used to compute the light intensity using the approach of Lehoczki et al.[1]
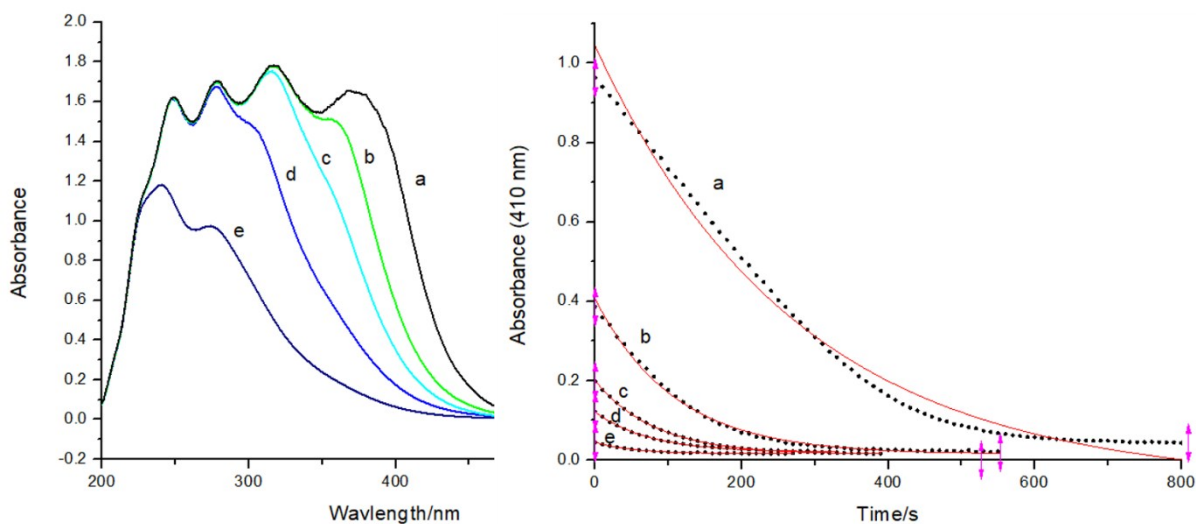

Fig. S7. Conversion **2** in 0.05 M H_2SO_4 at different concentrations and hence different absorbance at the irradiation wavelength. The initial spectra are shown on the left, and the corresponding time traces at 410 nm and a mono-exponential fit are shown on the right. The concentrations were adjusted that A'$_i$ = 3 (a), 1 (b), 0.5 (c), 0.3 (d) and 0.1 (e). The residuals of the fit from "a" to "e" are shown in Fig. S8.
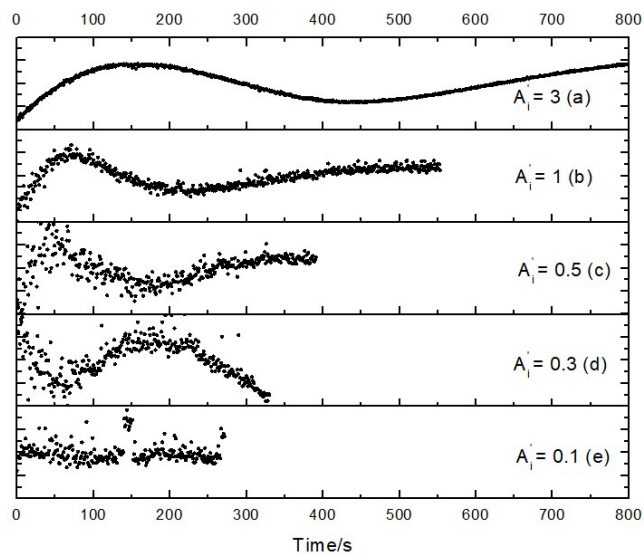
Fig. S8. Residuals for mono-exponential fits of solutions a, b, c, d and e shown in Fig. S6. When absorbance at the irradiation wavelength is below 0.1 (solution e) they can be described with a mono-exponential curve as indicated by random distributed residuals.

Ortho-nitrobenzaldehyde (**1**) as chemical actinometer

The absorbance at the irradiation wavelength (A'_i) was calculated by multiplying the concentration with the corresponding extinction coefficient at the irradiation wavelength (385 nm, ε = 68.7 ± 0.7 L·mol^{-1}·cm^{-1}). The extinction coefficient was determined by a calibration curve from five independent stock solutions to ensure a quantitative measurement. The graph is shown in Fig. S9. The reaction volume was corrected by using Equation S1.
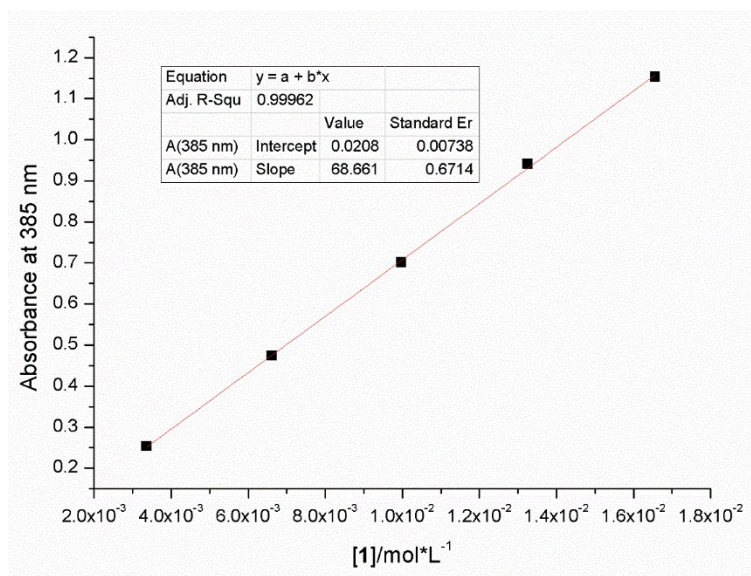

*Fig. S9. Calibration curve for **1** at the LED irradiation wavelength (385 nm).*
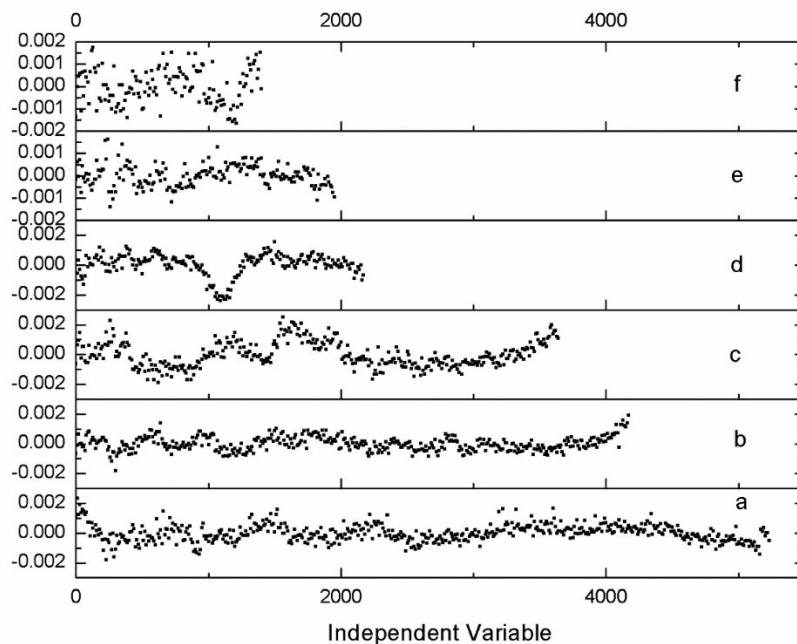
*Fig. S10. Residuals of the plot used to calculate the quantum yield for the conversion of **1** to **P1**. The letters denote the forward currents 5, 10,15, 20, 25 and 30 mA.*

As the quantum yield for the photo-conversion of **1** is known, it can be used as a chemical actinometer for photoreactions. By combining Equation 2 and Equation 8 and using the measured value of Φ = 0.43 the following expression for the LED output power is obtained:

$$P_{LED} = \frac{k_{fit}c_0 hcN_A V}{\Phi\lambda(1 - 10^{-A_i'})}$$

(S8)

In Equation S8, h is the Planck's constant (= $6.63 \cdot 10^{-34}$ J·s)*, c* is the speed of light in vacuum (= 299792458 m·s^{-1}), N_A is the Avogadro's constant (= $6.02 \cdot 10^{23}$) and Φ is the quantum yield for the conversion of **1** to **P1** (0.43 for irradiation at 385 nm). Experimental parameters are the peak wavelength λ of the LED (in m), the reaction volume V (in L), the decay constant k_{fit}, obtained by exponential fitting of the absorbance trace and the deployed concentration of **1**, c_0 (in mol·L^{-1}).

The values obtained with Equation S8 can be compared with the measured optical output of the LED and the values given in the LEDs data sheet (11 mW operated at 20 mA, assuming linear relation). A plot of current vs. the optical output in mW for all three methods is presented in Fig. S11.
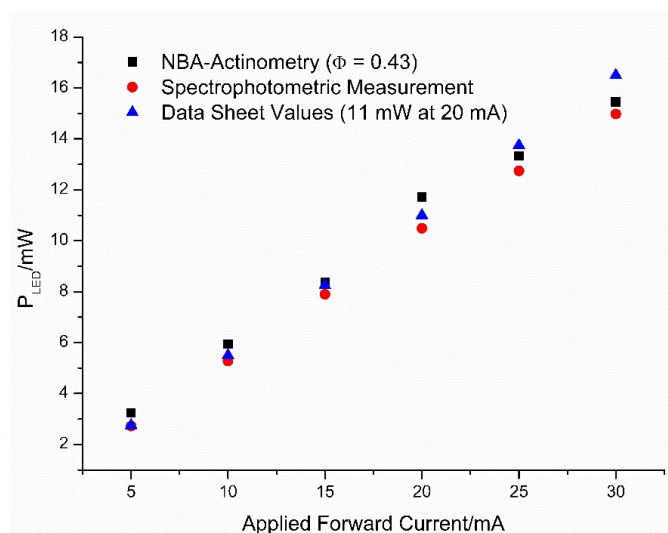
*Fig. S11. Output power for six LED operating currents. Black squares: values obtained by **1**-actinometry with Equation S8. Red circles: Spectrophotometric values measured before and after the experiment. Blue triangles: Output power given by the LEDs specifications, assuming linear behavior.*
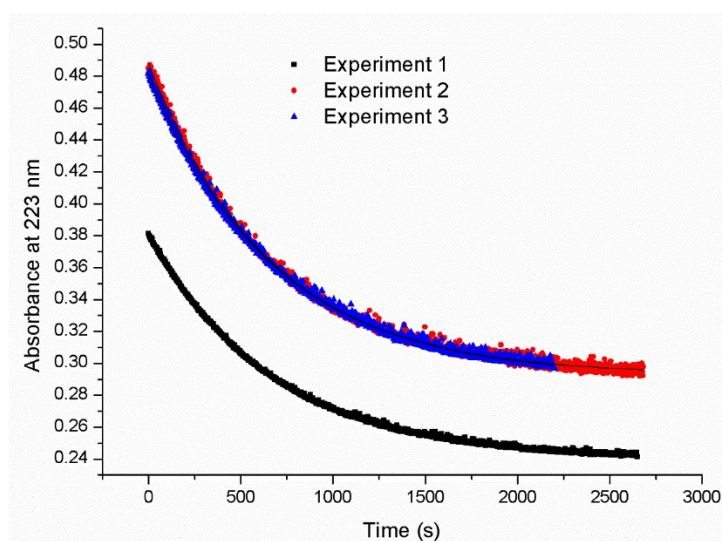
Control experiment with ferrioxalate

*Fig. S12. Three experiments with **1** irradiated with the same 385 nm LED operated at 20 mA referenced to ferrioxalate (see Table S4). The Figure displays experimental data and mono-exponential fitting functions listed in Table S2. The residuals of the fitting function are shown in in Figure S13. Sample details: 42 µM (Experiment 2 and 3) and 34 µM in acetonitrile, irradiated volume = 2 mL.*
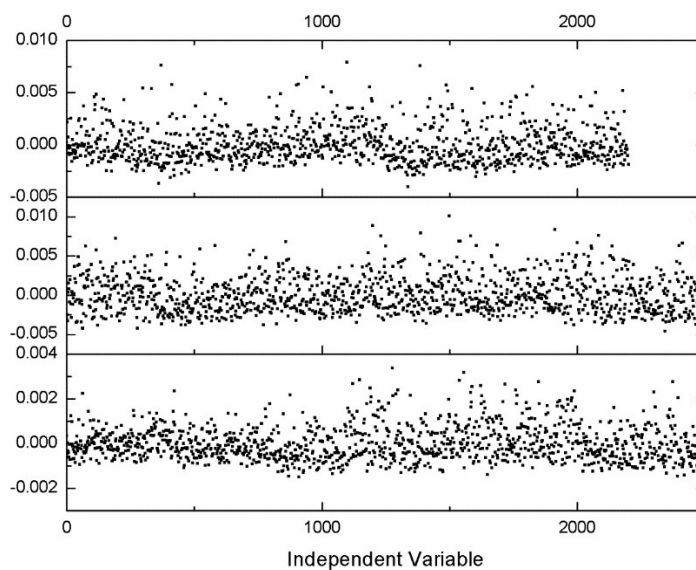
Fig. S13. Regular residuals of the mono-exponential fit presented in Figure S12 for experiment 1, 2 and 3 (bottom to top).

*Table S2. Quantum yield calculation for **1** irradiated at 385 nm in acetonitrile. In all cases the irradiated volume was 2 mL.*

sample	c_0 µM[a]	k_{fit} [s^{-1}]	reduced R^2	$A^{i,b}$	Φ^c
#1	33.5	$1.50 \cdot 10^{-3}$	0.99944	$2.24 \cdot 10^{-3}$	0.41
#2	42.4	$1.52 \cdot 10^{-3}$	0.99788	$2.84 \cdot 10^{-3}$	0.42
#3	42.4	$1.48 \cdot 10^{-3}$	0.99874	$2.84 \cdot 10^{-3}$	0.41
		Average: 0.42 ± 0.04^d			

[a]concentration calculated from the known concentration of two different stock solutions.

[b]calculated with the extinction coefficient at the irradiation wavelength

($\varepsilon_{385\,nm}$ = 68.7 L·mol^{-1}·cm^{-1}).

[c]using the light power determined with potassium ferrioxalate actinometry (see Fig. S16 and Table S4, P_{LED} = 14.3 mW).

[d]the error set to 10%. Error of Exp. #1- #3 is 0.005.

Actinometric measurements using ferrioxalate (2)

Following Lehóczki[1] *et al.* we use the quantum yield (ϕ = 1.2) and the extinction coefficient at the observation wavelength (410 nm, $\varepsilon_{obs.}$ = 146) to obtain the photon flow into the photo reactor.

$$I_0 = \frac{slope}{\varepsilon_{obs.}\phi}$$

(S9)

First we tested the linearity of this method in our conditions using ϕ = 1.2. Similar to **1** the current driving a 385 nm LED was varied from 5 to 30 mA. The light power was computed with Equation S9 and compared with values measured with the spectrophotometer using the geometry shown in Fig. S2.
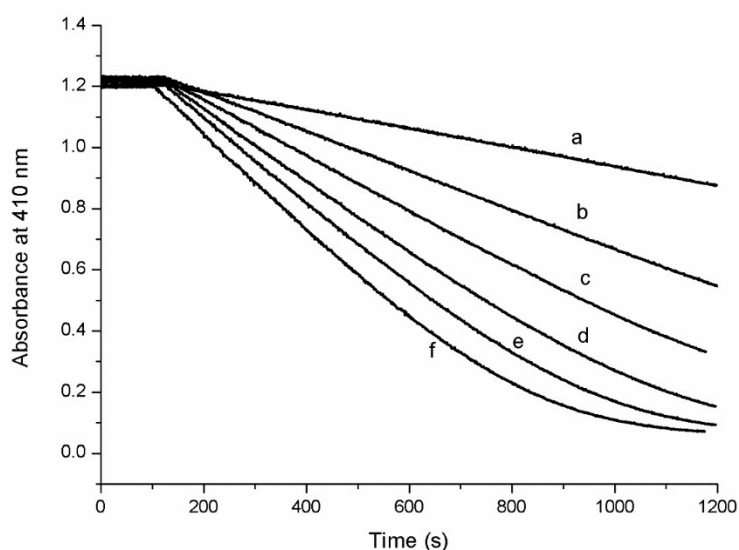

Fig. S14. 3 mL Ferrioxalate solutions (stock solution: 98.1 mg in 20 mL 0.05 M H_2SO_4, c = 11.2 mM, measurement volume = 3 mL) irradiated in the described setup with different forward currents of a 385 nm LED. Currents of 5, 10, 15, 20, 25 and 30 mA are denoted as a, b, c, d, e and f. Result of a linear fit of the first 100 data points (50 s irradiation time) is shown in Table S3.

Table S3. *Irradiation of six ferrioxalate solutions at different concentrations.*

trace in Figure S14	current /mA	slope (410 nm)/s^{-1}	optical light power/mW[a]	spectrophotometric determination[b]/mW	error[c]
a	5	5.97·10^{-4}	3.2	3.3	4%
b	10	1.27·10^{-3}	6.8	6.5	-4%
c	15	1.82·10^{-3}	9.7	9.5	-3%
d	20	2.36·10^{-3}	12.6	12.1	-5%
e	25	2.77·10^{-3}	14.7	14.2	-4%
f	30	3.12·10^{-3}	16.6	16.2	-3%

[b]five determinations after each ferrioxalate experiment with the geometry shown in Figure S2.

[a]the slope is converted to light power by fitting the first 100 data points and using ϕ = 1.2 and $\varepsilon_{obs.}$ = 146 (410 nm).

[c]with respect to the spectrophotometric determination, up-rounded values (*e.g.* entry d from 4.05 to 5%).
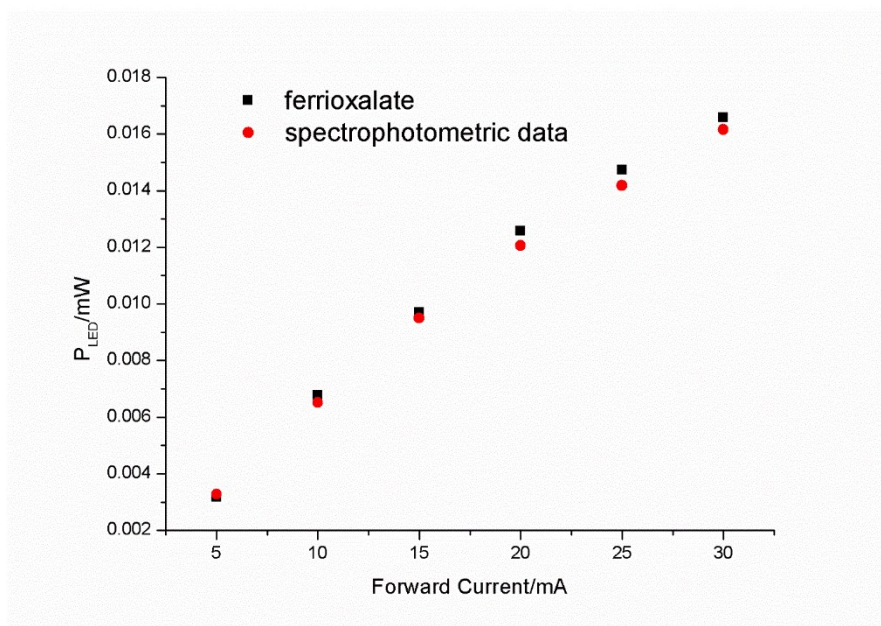

Fig. S15. *Graphical representation of the obtained light powers reported in Table S3.*

Good agreement between actinometric measurement and spectrophotometric determinations justifies the use of ϕ = 1.2 for 385 nm. Literature values are 1.14 for 405 nm and 1.21 for 365 nm and 1.26 for 365 nm.[1,2]

The 385 nm LED operated at 20 mA used for the quantum yield determination of compound **1**, **4** and **5** was measured using the above described formalism (Equation S9). The results of three measurements are shown in Table S4. The first 10 data points were noisy, therefore the slope in the range of 10 to 30 seconds (= 40 data

points at a sampling interval of 0.5 s) were used for fitting (insert Figure S16). The corresponding residuals are shown in Figure S17.

Table S4. Ferrioxalate experiment used to determine the photon flow of a 385 nm LED into the UV-Vis cuvette. The average value is used for the quantum yield determination of **1** and initiators **4** and **5**. Irradiated volume = 3 mL. Calculated with ϕ = 1.2 and $\varepsilon_{obs.}$ = 59 using Equation S9.

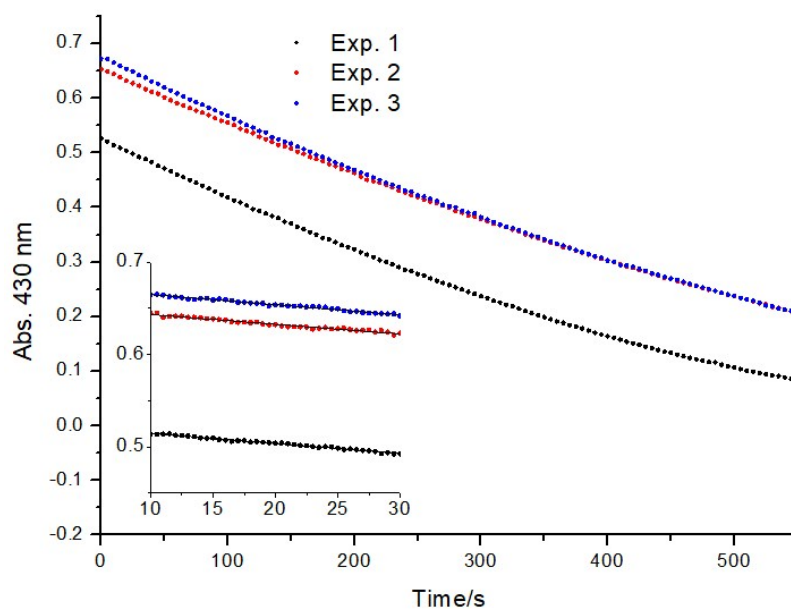|	slope at 430 nm /s^{-1}	R^2	I_0/mol·L^{-1}·s^{-1}
#1	1.09 ·10^{-3}	0.99	1.54·10^{-5}
#2	1.06 ·10^{-4}	0.97	1.50·10^{-5}
#3	1.10 ·10^{-3}	0.98	1.55·10^{-5}
Average:	(1.53 ± 0.03)·10^{-5} mol·L^{-1}·s^{-1}		(14.3 ± 0.3 mW)

Fig. S16. Absorbance traces at 430 nm used for ferrioxalate actinometry. The insert shows the region between 10 and 30 seconds in more detail, and the linear fits used to calculate the light intensity.
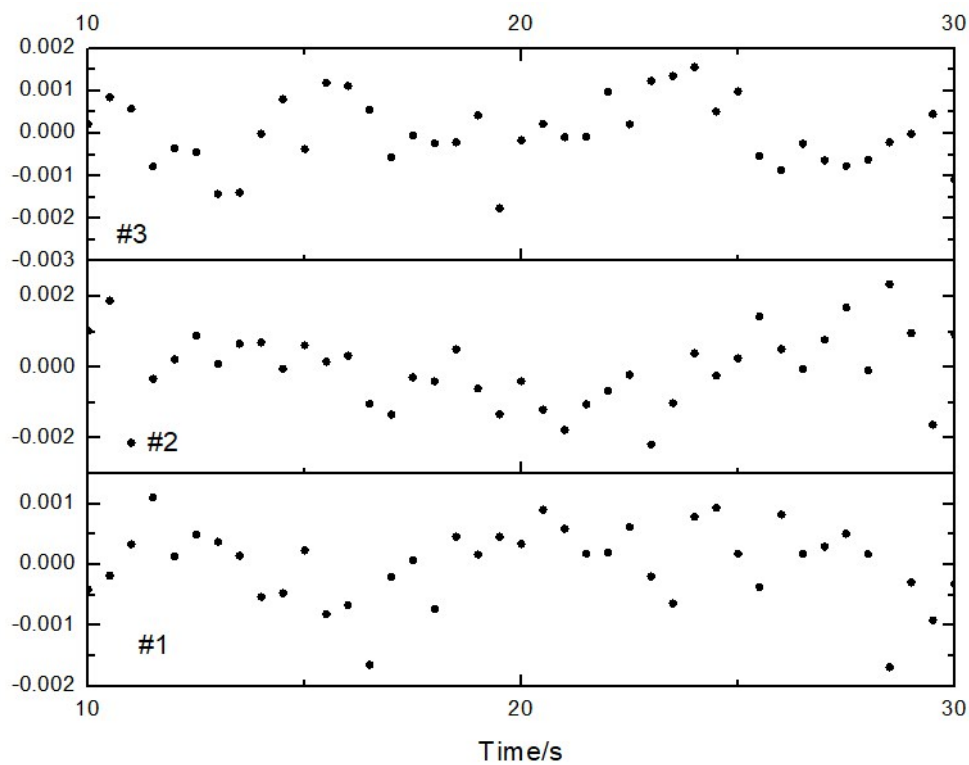
Fig. S17. Residuals for the linear fits used in Table S4 and shown in the insert of Fig. S16.
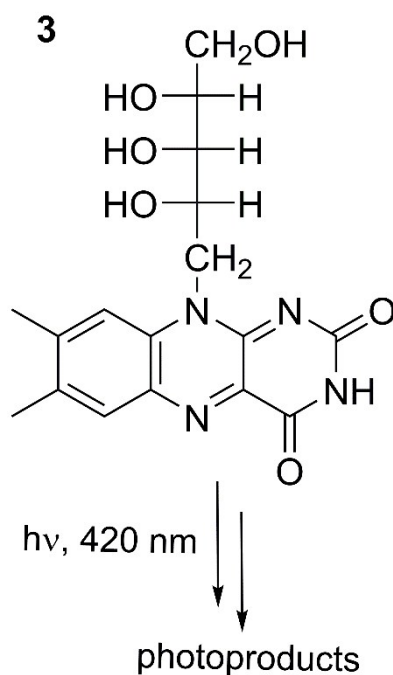
Photolysis of riboflavin (**3**)

Fig. S18. Structure of riboflavin (**3**).
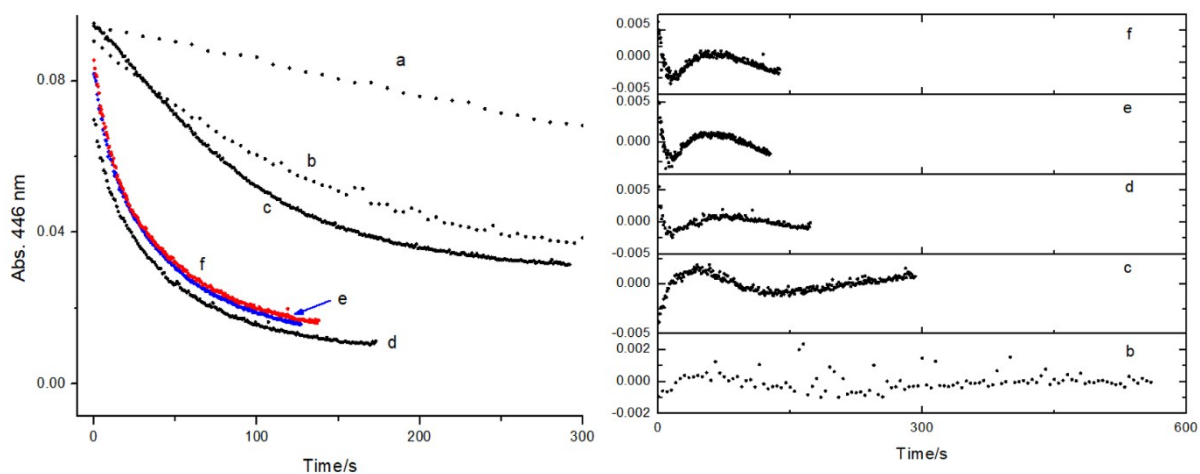
Fig. S19. Left: Absorbance traces monitored at 446 nm of 3 mL 7.7 µM riboflavin solutions in 0.01 M H_2SO_4 irradiated with a 420 nm LED (20 mA forward current). The solutions were bubbled with argon before the measurement for 0, 1, 2, 3, 4, 5 minutes, denoted by the letters a, b, c, d, e and f, respectively. Mono-exponential fits were used to extract time constants presented in Table S5. The residuals for b-f are shown on the right, the residuals for experiment "a" are displayed in Fig. 4 of the main text.

Table S5: Data presented in Fig. S19.

entry	argon bubbling	k_{fit} [s^{-1}]	R^2	$A^{i,a}$	apparent Φ^b
a	none	$1.64 \cdot 10^{-3}$	0.999	0.075	0.004
b	1 min.	$6.95 \cdot 10^{-3}$	0.998	0.076	0.019
c	2 min.	$1.04 \cdot 10^{-2}$	0.997	0.073	0.028
d	3 min.	$2.49 \cdot 10^{-2}$	0.994	0.069	0.068
e	4 min.	$2.96 \cdot 10^{-2}$	0.994	0.072	0.081
f	5 min.	$2.98 \cdot 10^{-2}$	0.992	0.074	0.082
Average of e and f: $\Phi = 0.08 \pm 0.008^c$					

[a]measured in triplicate before irradiation of the sample.
[b]using $I_0 = 1.75 \cdot 10^{-5}$ mol·L^{-1}·s^{-1} determined by three spectrophotometric measurements and using the gravimetrically determined concentration of 7.7 µM.
[c]set to 10 % since computing the standard deviation of e and f gave $3 \cdot 10^{-4}$.

Fig. S20 shows time resolved fluorescence spectra during the photo degradation of ca. 20 µM riboflavin solution under anaerobic conditions induced by a 385 nm LED. We used the spectrometer in emission mode with the light source for the spectrometer beam being switched off. While the fluorescence at 536 nm decreases the fluorescence emission at 456 nm increases. Fig. S20 b shows normalized time profiles of the fluorescence emission. Scattered LED light also reaches the detector.
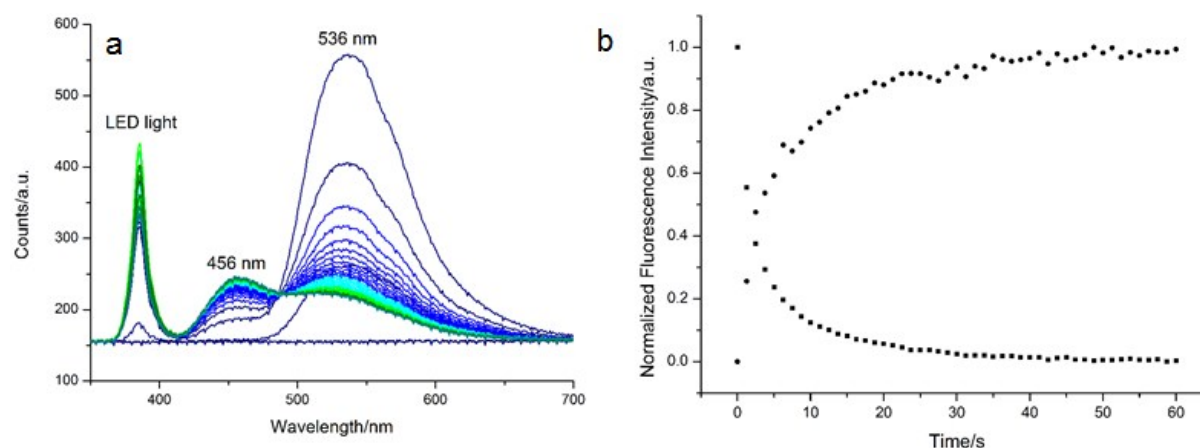

Fig. S20. Time Resolved Fluorescence spectra and scattered LED light recorded during photo-degradation (a). Normalized time profiles for the fluorescence intensity at 456 and 536 nm are shown left (b).

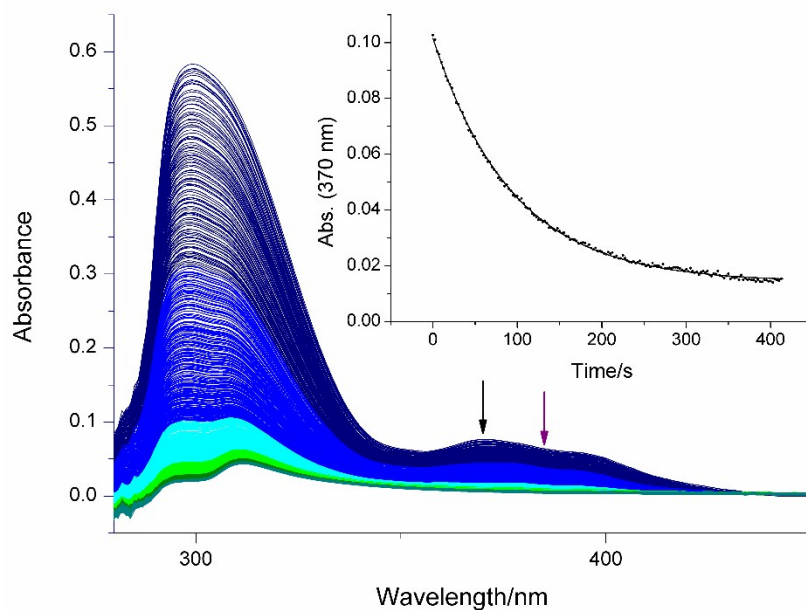# Cleavage of photoinitiators (**4** and **5**)

*Fig. S21. Spectra and trace monitored at 370 nm upon irradiation of 3 mL of 0.13 mM sample of initiator **4** in MMA/acetonitrile (1/1, v/v). The extracted data is presented in Table S6.*

*Table S6. Results for quantum yield determination of compound **4**, irradiated with 385 nm LED operated at 20 mA. Irradiated volume = 3 mL.*

sample	c mM[a]	k_{fit} [s^{-1}]	reduced R^2	A^{i}[b]	Φ[c]
#1	0.13	$1.13 \cdot 10^{-2}$	0.99913	$7.86 \cdot 10^{-2}$	0.56
#2	0.13	$1.20 \cdot 10^{-2}$	0.99968	$7.68 \cdot 10^{-2}$	0.61
#3	0.13	$1.21 \cdot 10^{-2}$	0.99982	$7.62 \cdot 10^{-2}$	0.62
			Average: 0.60 ± 0.03		

[a]concentration calculated from the known concentration of a stock solution (gravimetric).
[b]average of three absorbance measurements at 385 nm
[c]using the photon flux determined with potassium ferrioxalate actinometry (see Table S4, I_0 = $(1.53 \pm 0.03) \cdot 10^{-5}$ mol·L^{-1}·s^{-1}).
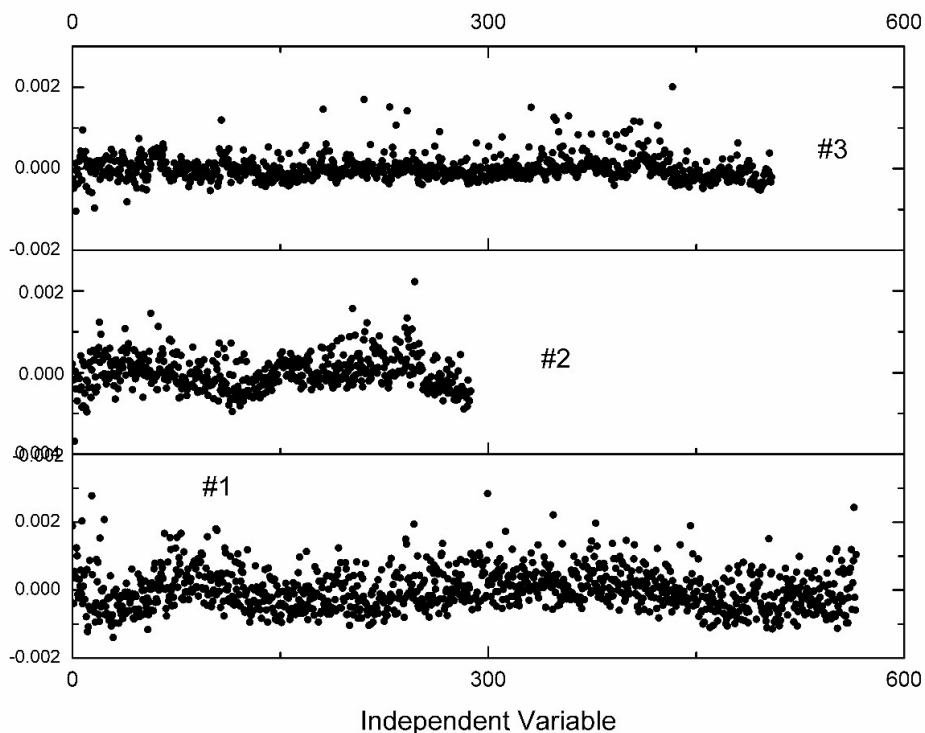
Fig. S22. Residuals for mono-exponential fitting of the data presented in Table S6 for entry 1-3 (bottom to top).

*Table S7. Results for quantum yield determination of compound **5**, irradiated with 385 nm LED operated at 20 mA. Irradiated volume = 3 mL.*

sample	c mM[a]	k_{fit} [s^{-1}]	reduced R^2	A^{i,b}	Φ^c
#1	0.17	$5.31 \cdot 10^{-2}$	0.99987	$3.20 \cdot 10^{-2}$	0.85
#2	0.17	$4.73 \cdot 10^{-2}$	0.9998	$3.32 \cdot 10^{-2}$	0.79
#3	0.17	$5.08 \cdot 10^{-2}$	0.99975	$3.20 \cdot 10^{-2}$	0.74
#4	0.17	$5.42 \cdot 10^{-2}$	0.99975	$3.12 \cdot 10^{-2}$	0.83
Average: 0.80 ± 0.04					

[a]concentration calculated from the known concentration of a stock solution (gravimetric).
[b]average of three absorbance measurements at 385 nm
[c]using the photon flux determined with potassium ferrioxalate actinometry (see Table S4, I_0 = $(1.53 \pm 0.03) \cdot 10^{-5}$ mol·L^{-1}·s^{-1}).
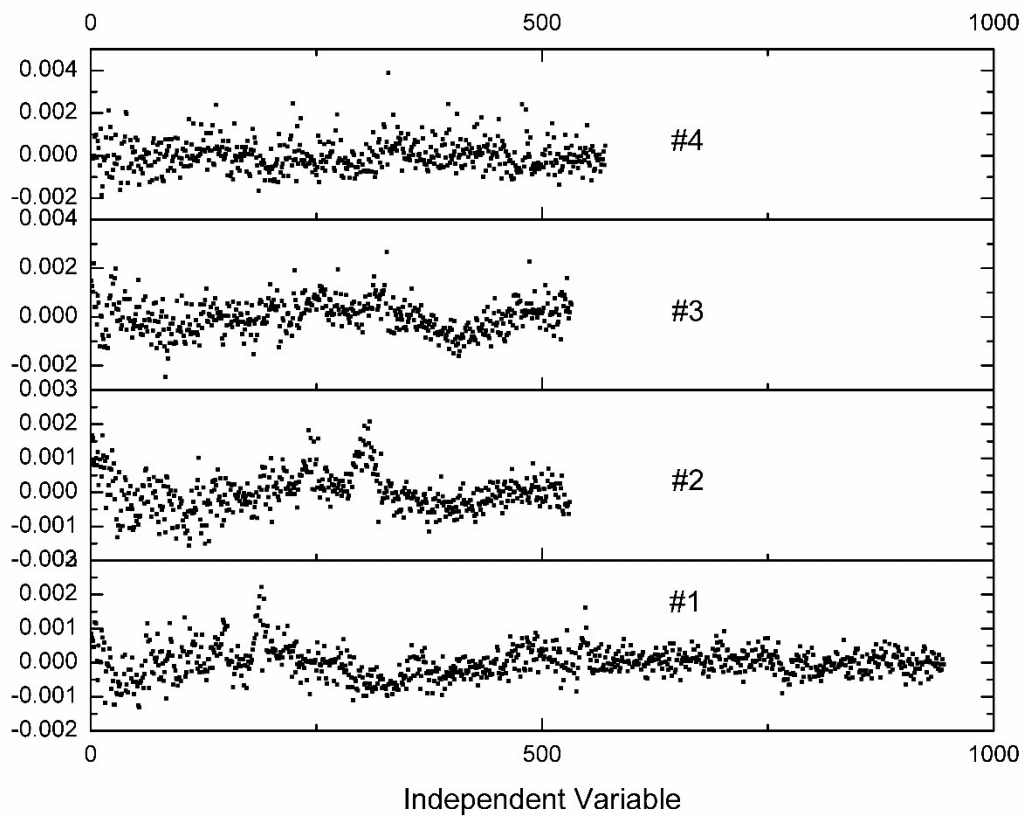
Fig. S23. Residuals of mono-exponential fitting of data presented in Table S7.

Color formation of a spirobenzopyran (6)

Under continuous irradiation with UV-light, a photo stationary state (PSS) is established. In the PSS no spectral changes are observable, it follows that the concentrations of species A (**6**) and B (**P6**) are constant, *i.e.* the rate of coloration and first order reverse reaction are equal. Figure S24 shows the absorbance trace at 569 nm (Spectra in main paper Figure 6).
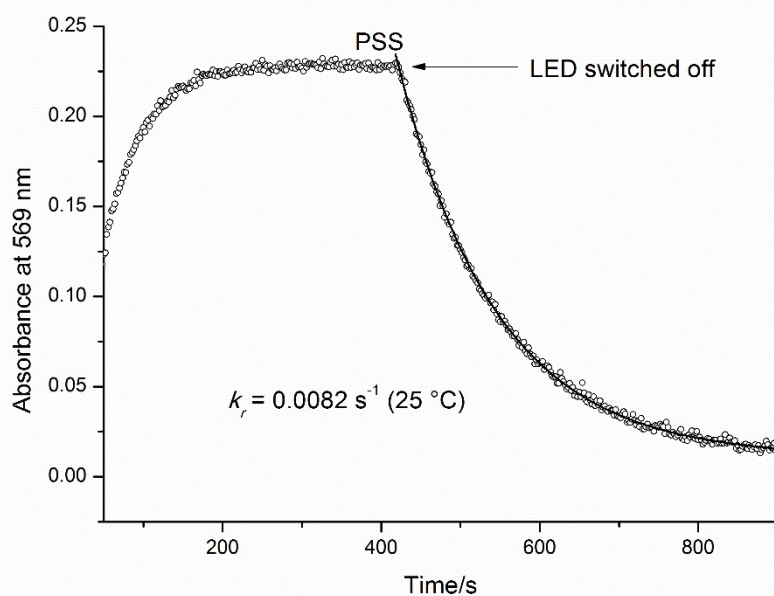

Fig. S24. Time profile of isomerization of compound **6**. In the PSS the absorbance is constant, switching the LED off allows to observe the characteristic first order reverse reaction.

Mathematically this condition is expressed with Equation S10.

$$I_0 F \varepsilon_A'[A]\Phi_c = [B](I_0 F \varepsilon_B'\Phi_r + k_r)$$

(S10)

I_0 is the light intensity (in mol·L⁻¹·s⁻¹), F is the photochemical factor, $F = (1 - 10^{-A'})/A'$ with A' being the absorbance at the irradiation wavelength, ε_A' and ε_B' are the molar extinction coefficients of species A and B at the irradiation wavelength (in L·mol⁻¹·cm⁻¹), Φ_c and Φ_r are the quantum yields for the photo isomerization and k_r is the rate constant for thermal reverse reaction (in s⁻¹). We express the concentration of species $[B]$ using the absorbance at 569 nm, $[B] = A_c/\varepsilon_{B.c}$. For very small light

intensities the conversion in the PSS is small and $k_r \gg I_0 F \varepsilon_B' \Phi_r$ and hence it follows that $I_0 F \varepsilon_B' \Phi_r + k_r \approx k_r$. Equation S10 then reads:

$$I_0 F \varepsilon_A'[A]\Phi_c = \frac{A_c}{\varepsilon_{B,c}}k_r \tag{S11}$$

Since the photo-chemical reaction is negligible compared to the thermal reverse reaction and turnover is very low, we assume that only species A absorbs the incident light. This assumption further simplifies the left side of Equation S11.

$$I_0(1 - 10^{A'})\Phi_c = \frac{A_c}{\varepsilon_{B,c}}k_r \tag{S12}$$

Since the quantum yield Φ_c and the precise extinction coefficient of species B (**P6**) is not known we have to use a range of literature values of $3.5 \cdot 10^4$ and $5.2 \cdot 10^4$ for $\varepsilon_{B,c}$ (569 nm), respectively.

The precise mechanism of the coloration of compound **6** has been studied in detail by Görner and coworkers.[3–7] The mechanism is shown in Figure S25.
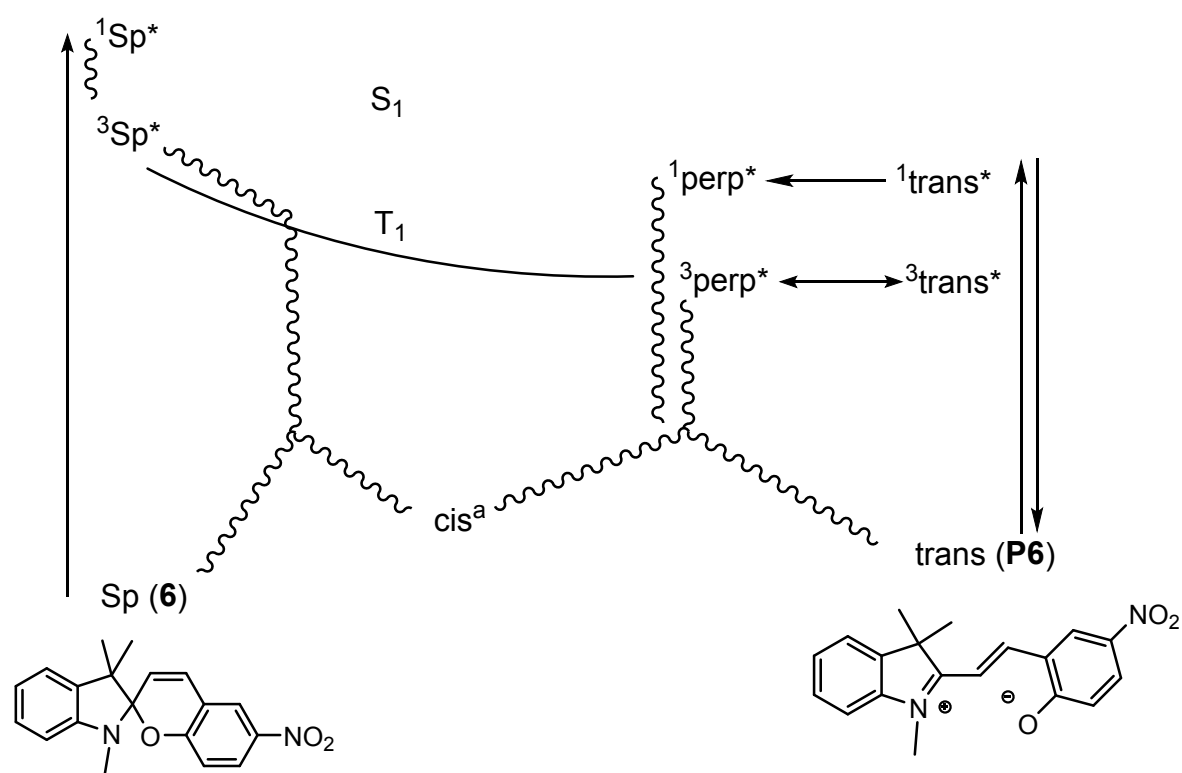

Fig. S25. Mechanism for coloration of compound **6**. Scheme adapted from references 2-7. Superscripts denote the spin multiplicity, S_1 and T_1 are the first excited singlet and triplet state, respectively. Perp: species with perpendicular geometry of the two aromatic rings. The LED light leads to excitation of thermodynamically more

stable isomer Sp (**6**) and its intensely colored trans form (**P6**) as indicated by vertical arrows. Curvy arrows indicate relaxation processes.

Isomerization of azobenzene (**7**)

Table S8. Determination of the photon flow of the used 400 nm LED operated at 20 mA into the UV-Vis cuvette. The average value is used for the determination of Q of azobenzene. Stock solution 140.2 mg in 10 mL 0.05 M H_2SO_4, c = 28.5 mM (entry 1-3) and 25.0 mg in 3 mL (entry #4). Irradiated volume = 3 mL, observation wavelength = 440 nm. Photon flux calculated with ϕ = 1.13 and $\varepsilon_{obs.}$ = 36.9 using Equation S9. The residuals of the fits resemble random noise.

	slope at 430 nm /s^{-1}	I_0/mol·L^{-1}·s^{-1}
#1	8.84 ·10^{-4}	2.13·10^{-5}
#2	8.68 ·10^{-4}	2.08·10^{-5}
#3	8.55 ·10^{-4}	2.05·10^{-5}
#4	9.16 ·10^{-4}	2.20·10^{-5}
Average:	(2.11 ± 0.06)·10^{-5} mol·L^{-1}·s^{-1}	(18.9 ± 0.5 mW)

Table S9. Isomerization of azobenzene followed by UV-Vis. Sample details: 0.12 mM azobenzene in 3 mL methanol. Irradiated with a 400 nm LED operated at 20 mA after irradiation with a high power UV-lamp. The absorbance was followed at 436 nm.

sample	k_{fit} [s^{-1}]	reduced R^2	A$^{i'a}$	F$^{i'}$	Q^c [L·mol^{-1}·cm^{-1}]
#1	2.06·10^{-2}	0.99784	8.93·10^{-2}	2.08	470
#2	2.06·10^{-2}	0.99667	8.40·10^{-2}	2.09	466
#3	2.01·10^{-2}	0.9969	8.59·10^{-2}	2.09	456
		Average: 464 ± 6 L·mol^{-1}·cm^{-1}			

[a]average of three absorbance measurements at 400 nm

[c]using the photon flux determined with potassium ferrioxalate actinometry (see Table S8, I_0 = (2.11 ± 0.06) ·10^{-5} mol·L^{-1}·s^{-1}).

References

1   T. Lehóczki, É. Józsa and K. Osz, Ferrioxalate actinometry with online spectrophotometric detection, *J. Photochem. Photobiol. A Chem.*, 2013, **251**, 63–68.

2   C. G. Hatchard and C. A. Parker, A New Sensitive Chemical Actinometer. II. Potassium Ferrioxalate as a Standard Chemical Actinometer, *Proc. R. Soc. A Math. Phys. Eng. Sci.*, 1956, **235**, 518–536.

3   H. Görner, Photochromism of nitrospiropyrans: effects of structure, solvent and temperature, *Phys. Chem. Chem. Phys.*, 2001, **3**, 416–423.

4   H. Görner, Photochemical ring opening in nitrospiropyrans: triplet pathway and the role of singlet molecular oxygen, *Chem. Phys. Lett.*, 1998, **288**, 589.

5   A. K. Chibisov and H. Görner, Photoprocesses in Spiropyran-Derived Merocyanines, *J. Phys. Chem. A*, 1997, **101**, 4305–4312.

6   A. K. Chibisov and H. Görner, Photoprocesses in Spiropyran-Derived Merocyanines, *J. Phys. Chem. A*, 1997, **101**, 4305–4312.

7   H. Görner, Photoprocesses in spiropyrans and their merocyanine isomers: Effects of temperature and viscosity, *Chem. Phys.*, 1997, **222**, 315–329.